Disturbance-Free Operation of Dual Three-Phase PM Machine Under Open-Phase Fault Considering Harmonic Current Injection

Lingling Guo, K. Wang, *Senior Member, IEEE*, Tao Wang, *Member, IEEE*, Ruiwu Cao, *Senior Member, IEEE*, and Feng Li

***Abstract*—This article proposes a full-order vector space decomposition (VSD) based fault-tolerant control with harmonic current injection for surface-mounted dual three-phase permanent magnet synchronous machine with open-phase fault to explore the limits of copper loss reduction and available torque improvement. Different from the conventional methods based on maintaining spatial circular rotation of magnetic motive force, the proposed method can achieve disturbance-free operation during open-phase fault only when *q*-axis current undisturbed, rather than requiring both *d*- and *q*-axis currents to be undisturbed. Thus, the degree of control freedom on *d*-axis can be released, where the simple harmonic current injection method can be employed to further improve fault-tolerant performance. Both theoretical and experimental results are presented to validate the superiority and effectiveness of the proposed method.**

***Index Terms*—Dual-three phase machine, fault-tolerant control, harmonic currents injection, maximum torque capability, minimum copper loss.**

I. Introduction

With the increasing requirements in high efficiency and high reliability, multiphase permanent magnet (PM) synchronous machine drives with inherent phase redundancy, which allow for continuous operation even under postfault, are highly appreciated at some modern industrial applications [1], [2]. However, unexpected malfunctions, such as, open-circuit faults, short-circuit faults, and sensor faults generally induce disturbances into the drive system, which degrades operation performance. To achieve disturbance-free operation, multiphase fault-tolerant control methods have been widely investigated [3], [4]. Since open-phase faults can act as remedies for many other fault types, existing fault-tolerant control methods mainly focus on open-phase faults.

For fault-tolerant control, the essence is to optimize and control the remaining healthy phase currents for both ensuring the average torque unchanged and minimizing the torque ripple [5], [6], [7]. However, multiphase machines still have additional degrees of freedom even under postfault, especially single open-phase faults, which leads to a higher number of unknowns than known conditions, so the solution for fault-tolerant currents is not unique. Generally, the minimum torque ripple is a common objective, beside which, two optional optimization objectives, namely, minimum loss (ML) and maximum torque (MT) can be selected to yield the optimal currents [8], [9].

To implement postfault vector control, several reduced-order vector space decomposition (VSD) matrixes have been developed for multi-phase machines with structural unbalance to obtain decoupling models. In [10], [11], and [12], the reduced-order VSD matrixes preserving the subspace orthogonality are developed for five-phase and dual three-phase (DTP) PM machines, respectively. In [13] and [14], the nonorthogonal reduced-order VSD matrix preserving the spatial circular rotation of PM flux linkage vector and magnetic motive force (MMF) is developed for five-phase PM machines, which provides the same mathematical model as the normal one. In [15], a simple reduced-order VSD matrix derived from the known optimal fault-tolerant current provides a remedial field-oriented control for open-circuit fault. Although both ML- and MT-based disturbance-free operation modes can be achieved through replacing the prefault matrix with the reduced-order ones, it requires feedforward voltage compensators or additional matrix to obtain decoupled *d-q* [10], [11], [12], [13], [14], [15]. Since reduced-order VSD matrix is different for each possible open-phase fault, in practice, either a large number of transformation matrices are required to be stored, or the phase order needs to be modified to use the same transformation matrix, which increases the complexity of control algorithm.

In addition to replacing the prefault matrix with the reduced-order ones, the case of preserving the prefault matrix has been already studied to avoid transformation matrix reconfiguration. For DTP machines with two three-phase winding configurations, the simplest fault-tolerant control is to remove the faulty three-phase winding containing the faulty phase when the prefault multiple three-phase VSD matrix is preserved [16].

Manuscript received 26 April 2023; revised 19 July 2023; accepted 1 August 2023. Date of publication 9 August 2023; date of current version 22 September 2023. This work was supported in part by the Regional Innovation and Development Joint Fund of the National Natural Science Foundation of China under Grant U22A20218, in part by the National Natural Science Foundation of China under Grant 52207058, and in part by the Postgraduate Research and Practice Innovation Program of Jiangsu Province under Grant KYCX21_0214. Recommended for publication by Associate Editor M. Hartmann. *(Corresponding author: K. Wang.)*

The authors are with the College of Automation Engineering, Nanjing University of Aeronautics and Astronautics, Nanjing 210016, China (e-mail: llingguo@nuaa.edu.cn; k_wang@ieee.org; wangtaoee@nuaa.edu.cn; ruiwucao@nuaa.edu.cn; lifeng988@nuaa.edu.cn).

Color versions of one or more figures in this article are available at https://doi.org/10.1109/TPEL.2023.3303434.

Digital Object Identifier 10.1109/TPEL.2023.3303434

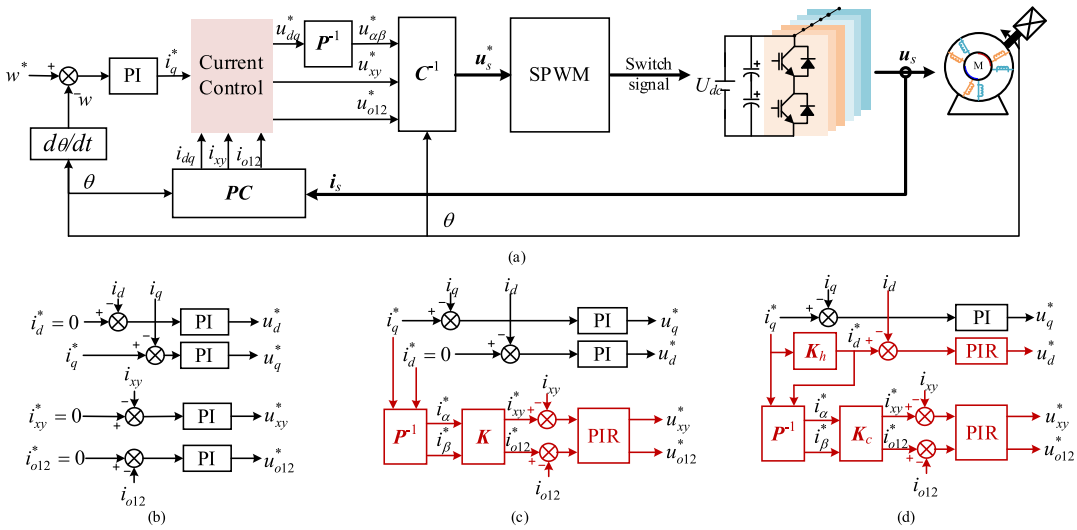

Fig. 1. (a) Vector control scheme under pre- and postfault. (b) Prefault decoupled current control. (c) Existing fault-tolerant control. (d) Proposed fault-tolerant control.

However, two healthy phases are disabled together with the faulty one, which causes significant reduction in the achievable power/torque. In [17] and [18], the influence of open-circuit fault on vector control is investigated when the prefault full-order VSD matrix is preserved. Fault-tolerant control can be achieved through maintaining the fundamental MMF undisturbed and then modifying loss-producing current references, as shown in Fig. 1(c). Due to the generality, it has been presented to improve the braking transients for six-phase induction machines with single open-phase fault in [19], evaluate postfault current/torque capability for symmetrical and asymmetrical six-phase machines under different fault types in [20], and achieve full-range ML for symmetrical multiphase machines under various fault conditions in [21]. However, the abovementioned methods are achieved based on undisturbed rotating MMF, where only the fundamental currents are considered. The reduction of copper loss and the improvement of torque capability under fault-tolerant operation are limited to some extent, as pointed out in this article.

To this end, disturbance-free operation considering harmonic current injection is investigated. In [22], the third harmonic current injection method is developed for further reducing copper loss of DTP machines with two isolated neutrals configuration under ML-based disturbance-free operation mode. Then, it is extended to MT mode for surface-mounted [23] and interior [24], [25] machines, respectively. However, due to the adoption of multiple three-phase VSD-based fault-tolerant control, the harmonic currents are only injected in the healthy three-phase winding, rather than all the remaining phases, which still limits the copper loss reduction and torque improvement. For surface-mounted machine, the smooth torque can be provided during open-phase faults when q-axis current is undisturbed. In [26], through releasing the demand on d-axis current, the optimal current is theoretically derived for DTP machines with single and two isolated neutrals configurations under ML-based disturbance-free operation mode. However, multiple complex functions are required to generate current references, increasing the complexity of fault-tolerant algorithm. Most importantly, it is difficult for the derivation-based method in [26] to be directly applied to MT mode with the multiple-objective characteristics, where the remaining phase currents should be optimized simultaneously to maximize torque per ampere. Hence, in [27], the particle swarm optimization algorithm is employed to yield the theoretical optimal current for MT mode. However, due to the high frequency characteristics of optimal current, it is difficult to guarantee the accurate injection.

As mentioned earlier, previous works related with harmonic injection either provide limited copper loss reduction or torque improvement due to the adoption of sinusoidal currents in faulty three-phase windings [22], [23], [24], [25], or inapplicable to MT mode due to the single-objective characteristics of analytical method [26], or fail to achieve the accurate injection due to high frequency characteristics of optimal current [27]. In this article, through investigating the influence of open-phase fault on vector control based on full-order VSD matrix, a simple method, which injects second and fourth harmonics into d-axis current while keeping the q-axis current undisturbed, is proposed for surface-mounted DTP machines with open-phase fault to explore the limits of copper loss reduction and torque capability improvement. Moreover, both theoretical and experimental results verify that the performance of the proposed method is comparable even better to the existing methods.

II. Influence of Open-Phase Fault on Vector Control

For DTP machine, the Clark transformation matrix can be expressed as

$$\boldsymbol{C} = \frac{1}{3}\begin{bmatrix} 1 & -\frac{1}{2} & -\frac{1}{2} & \frac{\sqrt{3}}{2} & -\frac{\sqrt{3}}{2} & 0 \\ 0 & \frac{\sqrt{3}}{2} & -\frac{\sqrt{3}}{2} & \frac{1}{2} & \frac{1}{2} & -1 \\ 1 & -\frac{1}{2} & -\frac{1}{2} & -\frac{\sqrt{3}}{2} & \frac{\sqrt{3}}{2} & 0 \\ 0 & -\frac{\sqrt{3}}{2} & \frac{\sqrt{3}}{2} & \frac{1}{2} & \frac{1}{2} & -1 \\ 1 & 1 & 1 & 0 & 0 & 0 \\ 0 & 0 & 0 & 1 & 1 & 1 \end{bmatrix}. \quad (1)$$

And the Park transformation matrix can be expressed as

$$\boldsymbol{P} = \begin{bmatrix} \cos\theta & \sin\theta \\ -\sin\theta & \cos\theta \end{bmatrix} \tag{2}$$

where θ is the rotor electrical angle.

The open-phase fault considered here is an open-circuit fault occurring in the connection at terminal of the machine, where the machine is not physically damaged. Thus, the machine mathematical model remains unchanged under pre- and postfault [18]. Through (1) and (2), the torque equation for surface-mounted machine to be tested can be expressed as

$$T_e = 3p\psi_f i_q \tag{3}$$

where p is the number of pole pairs and ψ_f is the amplitude of fundamental PM flux linkage.

When the open-phase fault occurs, the faulty phase current is zero, i.e., $i_f = 0$. Through inverse VSD transformation matrix, the following relationship is satisfied:

$$\begin{aligned} &i_d \cos(\theta - \varphi_f) - i_q \sin(\theta - \varphi_f) \\ &+ i_x \cos 5\varphi_f + i_y \sin 5\varphi_f \pm i_{o1} = 0 \end{aligned} \tag{4}$$

where the subscript $f \in \{a_1,b_1,c_1,a_2,b_2,c_2\}$ represents faulty phase and the corresponding faulty phase angle $\varphi_f \in \{0, 2\pi/3, -2\pi/3, \pi/6, 5\pi/6, -\pi/2\}$. For the last term on the right-hand side of the equation, the addition and subtraction operators are for $f \in \{a_1,b_1,c_1\}$ and $f \in \{a_2,b_2,c_2\}$, respectively. Here, i_{o2} is uniformly replaced by $-i_{o1}$ for $f \in \{a_2,b_2,c_2\}$, since $i_{o1}+i_{o2} = 0$ and $i_{o1} = i_{o2} = 0$ are for single and two isolated neutrals configurations, respectively.

From (4), it can be observed that the d-q, x-y, and o_1-o_2 currents are no longer decoupled from each other under postfault. However, prefault current control is designed to achieve independent goals since they are decoupled from each other under prefault, as shown in Fig. 1(b). Therefore, under postfault, the prefault decoupled current control leads to the conflicts between d-q and x-y-o_1-o_2 current controllers, which degrades the performance of q-axis current controller to some extent [28], [29]. From (3), the q-axis current tracking performance directly affect the torque performance.

III. Proposed Fault-Tolerant Control

In this section, the proposed fault-tolerant control with harmonic current injection, as shown in Fig. 1(d), is described in detail.

A. Disturbance-Free Operation Through Maintaining the Q-Axis Current Undisturbed

To yield smooth torque under postfault, it is necessary to maintain the q-axis current undisturbed, which can be expressed as follows:

$$i_q = c \tag{5}$$

where $c = T_e/3p\psi_f$ is a constant.

Fig. 2 shows the current trajectories on d-q and α-β subspaces of postfault disturbance-free operation, where both the orange dot and line indicate the special case $i_d = 0$, as shown in Fig. 1(c). From Fig. 2(b), the fact that the trajectory of α-β current should be circular is just a special case of postfault disturbance-free operation. The smooth torque can be obtained even when the trajectory of α-β currents is no longer circular.

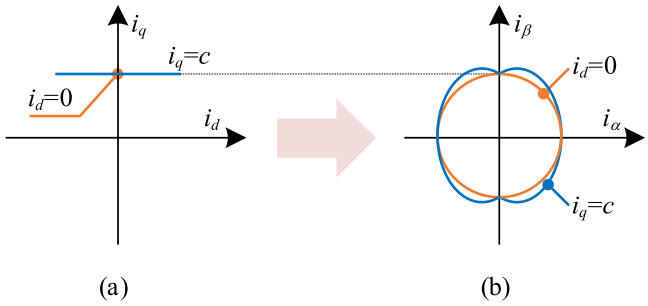

Fig. 2. Current trajectories on (a) d-q and (b) α-β subspace of postfault disturbance-free operation.

B. Fault-Tolerant Performance Improvement Through Injecting Harmonics Into D-Axis

Since the electromagnetic torque only relies on q-axis current, the requirement of postfault disturbance-free operation on d-axis current can be released to explore the limits of copper loss reduction and torque capability improvement. In this article, a simple alternative method is proposed to approach the optimal results through injecting harmonics into d-axis current.

As reported in [26], [27], [30], [31], and [32], third, fifth and even higher order harmonics (in stationary frame) have been utilized to improve control performance under healthy state and even fault-tolerant state. However, the requirement on control bandwidth increases as the harmonic order increases, while the potential benefit reduces [33], [34]. Thus, only third and fifth harmonics are considered here, which are mapped into the second and fourth harmonics at d-q synchronous frame. Based on the above analysis, d-axis current can be expressed as

$$i_d = i_q \left(k_{d2} sin(2\theta + \varphi_{d2}) + k_{d4} sin(4\theta + \varphi_{d4})\right) \tag{6}$$

where k_{d2} and k_{d4} are injection coefficients for second and fourth harmonics, respectively. φ_{d2} and φ_{d4} are the offset angles for second and fourth harmonics, respectively.

C. Decoupled Current Control Through Modifying x-y-o_1-o_2 Current References

Due to the additional constraints (4) introduced by faults, there is a conflict between the independent goals of current controllers and the fact that the actual current is coupled. For d-q current control to be effective, it is necessary to modify x-y-o_1-o_2 current references under postfault to decouple d-q current from them.

To obtain x-y-o_1-o_2 current references, (4) can be rewritten as

$$i_\alpha \cos\varphi_f + i_\beta \sin\varphi_f + i_x \cos 5\varphi_f + i_y \sin 5\varphi_f \pm i_{o1} = 0 \tag{7}$$

where i_α and i_β can be obtained through (2), (5), and (6), their detailed expressions are as follows

$$\begin{cases} i_\alpha = i_q \left[-\sin\theta + \frac{k_{d2}}{2}\left\{\sin\left(\theta+\varphi_{d2}\right)+\sin\left(3\theta+\varphi_{d2}\right)\right\} \right. \\ \qquad \left. +\frac{k_{d4}}{2}\left\{\sin\left(3\theta+\varphi_{d4}\right)+\sin\left(5\theta+\varphi_{d4}\right)\right\}\right] \\ i_\beta = i_q \left[\cos\theta + \frac{k_{d2}}{2}\left\{\cos\left(\theta+\varphi_{d2}\right)-\cos\left(3\theta+\varphi_{d2}\right)\right\} \right. \\ \qquad \left. +\frac{k_{d4}}{2}\left\{\cos\left(3\theta+\varphi_{d4}\right)-\cos\left(5\theta+\varphi_{d4}\right)\right\}\right]. \end{cases} \tag{8}$$

From (7), under postfault, x-y and o_1-axis currents can be expressed as the linear combination of α-β currents

$$\begin{cases} i_x = k_{11}\, i_\alpha + k_{12} i_\beta \\ i_y = k_{21}\, i_\alpha + k_{22} i_\beta \\ i_{o1} = k_{31}\, i_\alpha + k_{32} i_\beta \end{cases} \tag{9}$$

where $k_{11}, k_{12}, k_{21}, k_{22}, k_{31}$, and k_{32} are correlation coefficients. They satisfy the following relationship:

$$\begin{cases} \cos\varphi_f + k_{11}\cos 5\varphi_f + k_{21}\sin 5\varphi_f \pm k_{31} = 0 \\ \sin\varphi_f + k_{12}\cos 5\varphi_f + k_{22}\sin 5\varphi_f \pm k_{32} = 0. \end{cases} \tag{10}$$

Specially, for two isolated neutrals configuration, it meets the following relationship:

$$\begin{cases} k_{31} = 0 \\ k_{32} = 0 \end{cases}. \tag{11}$$

D. Selection of Optimal Coefficient

According to the previous analysis, there exist ten unknown variables (k_{d2}, k_{d4}, φ_{d2}, φ_{d4}, k_{11}, k_{12}, k_{21}, k_{22}, k_{31}, and k_{32}) and two/four equations described in (10) and/or (11), resulting in the multiple solutions. Here, two different disturbance-free operation modes are considered to yield optimal solutions.

1) ML Mode: The objective is to minimize stator copper loss, whose per unit value can be expressed as

$$p_{cu} = \left(\frac{1}{2\pi}\int_0^{2\pi}\sum_n i_n^2 d\theta\right)/3i_q^2 \tag{12}$$

where per-phase current can be expressed as

$$i_n = i_\alpha \cos\varphi_n + i_\beta \sin\varphi_n + i_x \cos 5\varphi_n + i_y \sin 5\varphi_n \pm i_{o1} \tag{13}$$

where the subscript $n \in \{a_1, b_1, c_1, a_2, b_2, c_2\}$ and the corresponding phase angle $\varphi_n \in \{0, 2\pi/3, -2\pi/3, \pi/6, 5\pi/6, -\pi/2\}$.

Substituting (8), (9), and (13) into (12), the normalized stator copper loss can be simplified as

$$p_{cu} = w_\alpha\, I_\alpha + w_\beta I_\beta + w_m I_m \tag{14}$$

with

$$\begin{cases} I_\alpha = \frac{1}{4}\left\{\begin{matrix} k_{d2}^2 + k_{d4}^2 + 2 - 2k_{d2}\cos\left(\varphi_{d2}\right) \\ +k_{d2}k_{d4}\cos\left(\varphi_{d2}-\varphi_{d4}\right) \end{matrix}\right\} \\ I_\beta = \frac{1}{4}\left\{\begin{matrix} k_{d2}^2 + k_{d4}^2 + 2 + 2k_{d2}\cos\left(\varphi_{d2}\right) \\ -k_{d2}k_{d4}\cos\left(\varphi_{d2}-\varphi_{d4}\right) \end{matrix}\right\} \\ I_m = \frac{1}{4}\left\{\begin{matrix} 2k_{d2}\sin\left(\varphi_{d2}\right) \\ +k_{d2}k_{d4}\sin\left(\varphi_{d2}-\varphi_{d4}\right) \end{matrix}\right\} \\ w_\alpha = 1 + k_{11}^2 + k_{21}^2 + 2k_{31}^2 \\ w_\beta = 1 + k_{12}^2 + k_{22}^2 + 2k_{32}^2 \\ w_m = 2\left(k_{11}k_{12} + k_{21}k_{22} + 2k_{31}k_{32}\right). \end{cases} \tag{15}$$

2) MT Mode: The objective is to maximize torque per ampere, which is equivalent to minimizing the maximum root mean square (rms) current at given torque.

For per-phase current, its normalized rms value can be expressed as

$$I_n = \sqrt{\frac{1}{2\pi}\int_0^{2\pi} i_n^2 d\theta}\Big/\left(\sqrt{2}i_q/2\right). \tag{16}$$

Substituting (8), (9), and (13) into (16), the normalized rms value can be simplified as

$$I_n = \sqrt{2\left(w_{n\alpha} I_\alpha + w_{n\beta} I_\beta + w_{nm} I_m\right)} \tag{17}$$

with

$$\begin{cases} w_{n\alpha} = \left(\cos\varphi_n + k_{11}\cos 5\varphi_n + k_{21}\sin 5\varphi_n \pm k_{31}\right)^2 \\ w_{n\beta} = \left(\sin\varphi_n + k_{12}\cos 5\varphi_n + k_{22}\sin 5\varphi_n \pm k_{32}\right)^2 \\ w_{nm} = 2\left(\cos\varphi_n + k_{11}\cos 5\varphi_n + k_{21}\sin 5\varphi_n \pm k_{31}\right) \\ \qquad \times\left(\sin\varphi_n + k_{12}\cos 5\varphi_n + k_{22}\sin 5\varphi_n \pm k_{32}\right). \end{cases} \tag{18}$$

Then, the maximum rms current can be expressed as

$$I_{\text{rms}} = max\left\{I_{a1}, I_{b1}, I_{c1}, I_{a2}, I_{b2}, I_{c2}\right\}. \tag{19}$$

As for torque capability, it is generally expressed as the ratio of maximum rms current of healthy state to that of fault-tolerant state [26], [27]. Since the maximum rms current (19) is normalized with respect to that of healthy state, the maximum torque capability at given rms current can be simplified as

$$T_{\text{MAX}} = 1/I_{\text{rms}} \times 100\%. \tag{20}$$

For ML and MT modes, the optimization objective is to minimize (14) and (19), respectively, and both are subjected to the restrictions as in (10). In particular, there are additional constraints (11) for two isolated neutrals configuration. With the help of MATLAB Optimization Toolbox in Appendix, the optimal coefficients are obtained and listed in Tabel I, which is applicable to any surface-mounted DTP machines and throughout the full operation regions since the optimization procedure does not involve any machine parameters and those parameters related operation states (speed and load). Moreover, Figs. 3–6 show optimal current waveforms on d-q-x-y(-o_1) and a_1-b_1-c_1-a_2-b_2-c_2 reference frames for different disturbance-free operation modes and different neutral point configurations. Fig. 7 shows current trajectories on α-β reference frame, where the trajectory of α-β currents is no longer circular, especially in MT mode.

TABLE I
OPTIMAL COEFFICIENTS FOR ML AND MT MODES WITH DIFFERENT NEUTRAL POINT CONFIGURATIONS

Neutrals	Mode	Faulty Phase	$\boldsymbol{K}_c$						$\boldsymbol{K}_h$			
			k_{11}	k_{12}	k_{21}	k_{22}	k_{31}	k_{32}	k_{d2}	k_{d4}	φ_{d2}	φ_{d4}
Single isolated	ML	a_1	-0.67	0	0	0	-0.33	0	0.25	-0.03	0	0
		b_1	-0.17	0.29	-0.29	0.50	0.17	-0.29	-0.25	0.03	-π/3	π/3
		c_1	-0.17	-0.29	0.29	0.50	0.17	0.29	-0.25	0.03	π/3	-π/3
		a_2	0.5	0.29	-0.29	-0.17	0.29	0.17	0.25	0.03	-π/3	π/3
		b_2	0.5	-0.29	0.29	-0.17	-0.29	0.17	0.25	0.03	π/3	-π/3
		c_2	0	0	0	-0.67	0	-0.33	-0.25	-0.03	0	0
	MT	a_1	-0.72	0	-0.38	-0.14	-0.28	0	0.51	-0.07	-π/10	π/10
		b_1	0.09	0.09	-0.47	0.66	0.13	-0.25	-0.51	0.07	-13π/30	13π/30
		c_1	-0.23	-0.66	0.27	0.34	0.15	0.24	-0.51	0.07	7π/30	-7π/30
		a_2	0.34	0.27	-0.66	-0.23	0.24	0.15	0.51	0.07	-7π/30	7π/30
		b_2	0.66	-0.47	0.09	0.09	-0.25	0.13	0.51	0.07	13π/30	-13π/30
		c_2	-0.14	-0.38	0	-0.72	0	-0.28	-0.51	-0.07	π/10	-π/10
Two isolated	ML	a_1	-1	0	0	0	0	0	0.34	-0.06	0	0
		b_1	-0.25	0.43	-0.43	0.75	0	0	-0.34	0.06	-π/3	π/3
		c_1	-0.25	-0.43	0.43	0.75	0	0	-0.34	0.06	π/3	-π/3
		a_2	0.75	0.43	-0.43	-0.25	0	0	0.34	0.06	-π/3	π/3
		b_2	0.75	-0.43	0.43	-0.25	0	0	0.34	0.06	π/3	-π/3
		c_2	0	0	0	-1	0	0	-0.34	-0.06	0	0
	MT	a_1	-1	0	0	-0.07	0	0	0.75	-0.25	0	0
		b_1	-0.2	0.46	-0.46	0.73	0	0	-0.75	0.25	-π/3	π/3
		c_1	-0.2	-0.46	0.46	0.73	0	0	-0.75	0.25	π/3	-π/3
		a_2	0.73	0.46	-0.46	-0.2	0	0	0.75	0.25	-π/3	π/3
		b_2	0.73	-0.46	0.46	-0.2	0	0	0.75	0.25	π/3	-π/3
		c_2	-0.07	0	0	-1	0	0	-0.75	-0.25	0	0

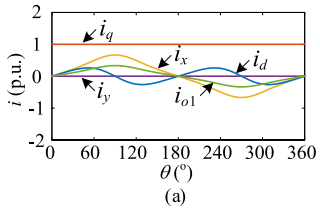

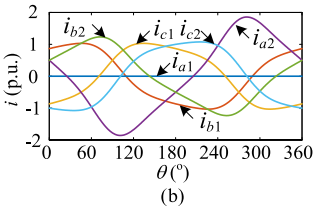

Fig. 3. ML-based current waveforms on (a) d-q-x-y-o_1 and (b) a_1-b_1-c_1-a_2-b_2-c_2 reference frames for a_1-phase open-phase fault under single isolated neutral configuration.

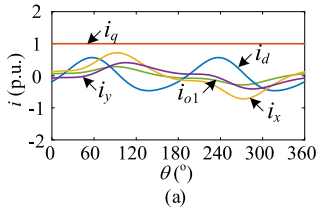

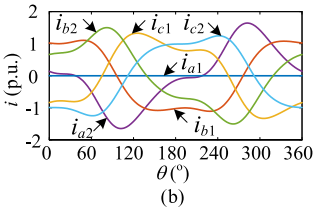

Fig. 4. MT-based current waveforms on (a) d-q-x-y-o_1 and (b) a_1-b_1-c_1-a_2-b_2-c_2 reference frames for a_1-phase open-phase fault under single isolated neutral configuration.

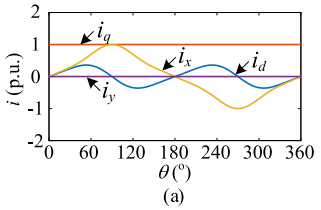

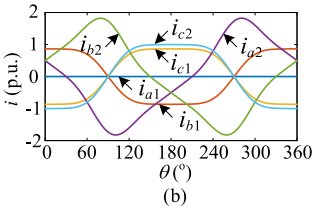

Fig. 5. ML-based current waveforms on (a) d-q-x-y and (b) a_1-b_1-c_1-a_2-b_2-c_2 reference frames for a_1-phase open-phase fault under two isolated neutrals configuration.

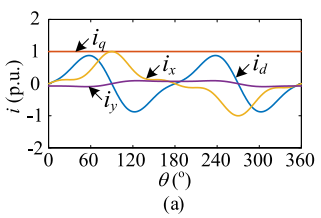

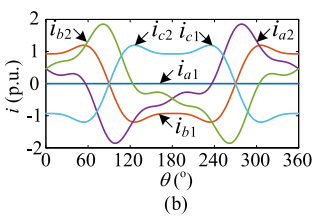

Fig. 6. MT-based current waveforms on (a) d-q-x-y and (b) a_1-b_1-c_1-a_2-b_2-c_2 reference frames for a_1-phase open-phase fault under two isolated neutrals configuration.

E. Fault-Tolerant Performance Comparison

To demonstrate the superiority of the proposed method, it is compared with previous works [18], [22], [23], [26], [27]. Table II lists the comparison results, where the copper loss, rms current, and torque capability are calculated by (12), (19), and (20), respectively. It can be seen from Table II that compared to M0, M1, and M3 methods in [18], [22], and [23], the proposed M5 method provides the lower copper loss and higher torque capability, even under different neutral point configurations and different disturbance-free operation modes. Compared to M2 and M4 methods in [26] and [27], the proposed M5 method provides the similar copper loss and torque capability through low-order harmonics and simple linear operations, as shown in (6) and (9), instead of those high frequencies or complex functions required in [26] and [27]. Table III lists the comparison results in terms of the selected harmonic orders, applicable

TABLE II
COMPARISON RESULTS OF COPPER LOSS, RMS CURRENT, AND TORQUE CAPABILITY

Method	Stator copper loss p_{cu} (p.u.)				Maximum rms current I_{rms} (p.u.)				Torque capability T_{MAX}			
	N1		N2		N1		N2		N1		N2	
	ML	MT	ML	MT	ML	MT	ML	MT	ML	MT	ML	MT
Healthy state	1				1				100			
M0 [18]	1.33	1.73	1.5	2	1.85	1.44	1.8	1.73	54.05%	69.44%	55.56%	57.8%
M1 [22]	-	-	1.43	-	-	-	1.62	-	-	-	61.73%	-
M2 [26]	**1.29**	-	**1.41**	-	1.67	-	1.57	-	60.24%	-	63.69%	-
M3 [23]	-	-	-	1.57	-	-	-	1.47	-	-	-	68.03%
M4 [27]	-	-	-	1.52	-	-	-	**1.37**	-	-	-	**72.99%**
Proposed M5	**1.29**	1.4	**1.41**	1.56	1.67	**1.3**	1.57	**1.37**	60.24%	**76.92%**	63.69%	**72.99%**

Note: M0 is the fault-tolerant method without harmonic injection, while M1–M5 with different harmonic injection. (b) N1 and N2 indicate single and two isolated neutrals configuration, respectively. (c) – indicates that the index is not provided.

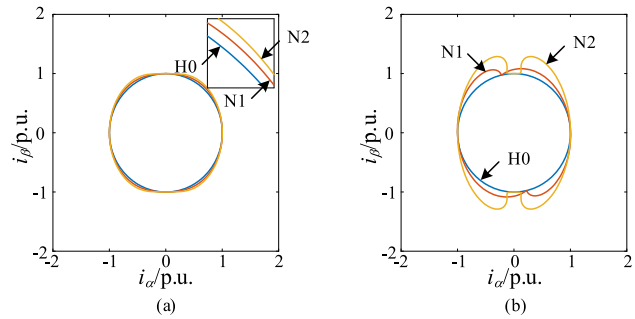

Fig. 7. Current trajectories on α-β subspace for (a) ML mode (b) MT mode, where H0, N1, N2 indicate healthy condition, single, and two isolated neutrals configuration, respectively.

TABLE III
COMPARISON RESULTS OF THE SELECTED HARMONIC ORDERS, APPLICABLE DISTURBANCE-FREE OPERATION MODES, AND NEUTRAL POINTS CONFIGURATIONS

Method	Harmonic order	Mode	Configurations
M0 [18]	1	ML,MT	N1,N2
M1 [22]	1,3 (healthy three-phase	ML	N2
M3 [23]	windings)	MT	N2
M2 [26]	1,3,5	ML	N1,N2
M4 [27]	1,3,5,7,9,…	MT	N2
Proposed M5	1,3,5	ML,MT	N1,N2

Note: N1 and N2 indicate single and two isolated neutrals configuration, respectively.

disturbance-free operation modes, and neutral points configurations. It should be noted that M2 and M4 methods only focus on one operation mode, while the proposed method provides a unified way to selectively implement ML or MT modes with only modification of the coefficients, regardless of single, or two isolated neutrals configurations.

IV. EXPERIMENTAL RESULTS

To validate the effectiveness of the proposed fault-tolerant control, an experimental platform based on dSPACE1007 is constructed, as shown in Fig. 8. The DTP machine, which is supplied by two two-level three-phase voltage source inverters (Mitsubishi PM300RL1A060) with parallel-connected dc-link, is coupled with a dc motor as the load. The phase current and torque are measured in real time through Hall effect sensors (CSM100B) and torque transducer (HBM T20WN), respectively. The key parameters of experimental setup are listed in Table IV.

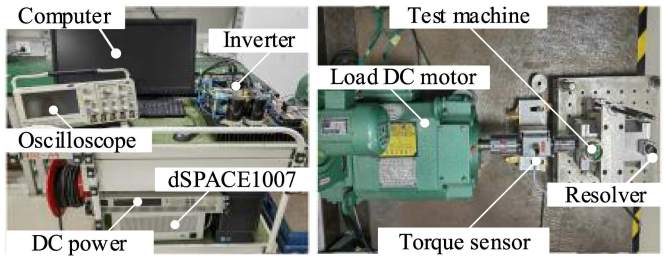

Fig. 8. Experimental platform.

TABLE IV
KEY PARAMETERS OF EXPERIMENTAL SETUP

Parameter	Value(unit)	Parameter	Value(unit)
Pole pairs	5	Stator resistance	0.7 Ω
d-q inductance	1.2 mH	x-y inductance	0.5 mH
PM flux-linkage	0.06 Wb	Switching frequency	10 kHz
Sampling frequency	10 kHz	Dc link voltage	80 V
Power	600 W	Rated load	6 N·m
Rated speed	1000 r/min	Rated current	10 A

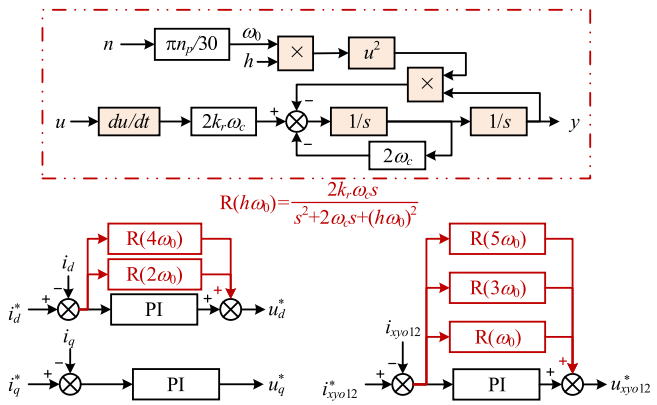

Fig. 9. Control block of current controllers.

In the experiments, the current controllers shown in Fig. 9 are employed to track the d-q-x-y-o_1-o_2 current references, where the resonant controller (red box) is only active under fault-tolerant operation. According to d-axis current reference

TABLE V
PARAMETERS OF SPEED AND CURRENT CONTROLLERS

Controller		Parameter		
		k_p	k_i	k_r
Speed controller		0.01	1	-
Current controller	q-axis current	0.1	1000	-
	d-axis current	0.1	1000	0.05
	x-y-o_1-o_2 current	0.3	1000	0.05

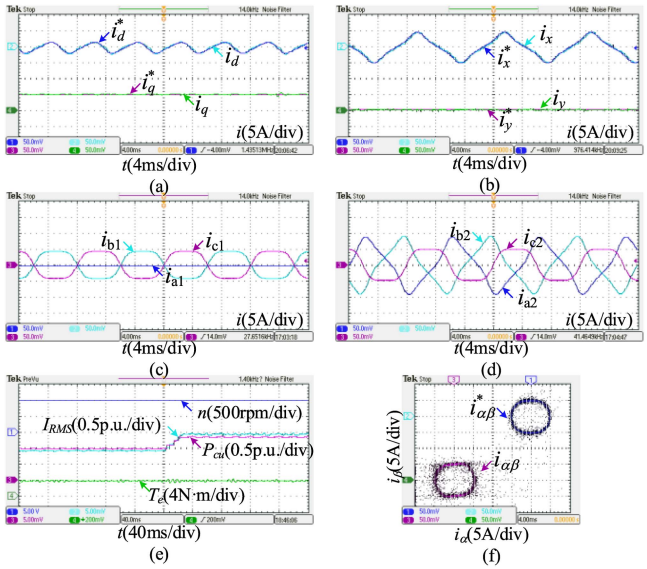

Fig. 10. ML-based experimental results for two isolated neutrals configuration. Current waveforms on (a) d-q subspace; (b) x-y subspace; (c) a_1-b_1-c_1 reference frame; (d) a_2-b_2-c_2 reference frame; (e) speed, torque, copper loss, and maximum rms current waveforms under healthy state and fault-tolerant state; (f) current trajectory on α-β subspace.

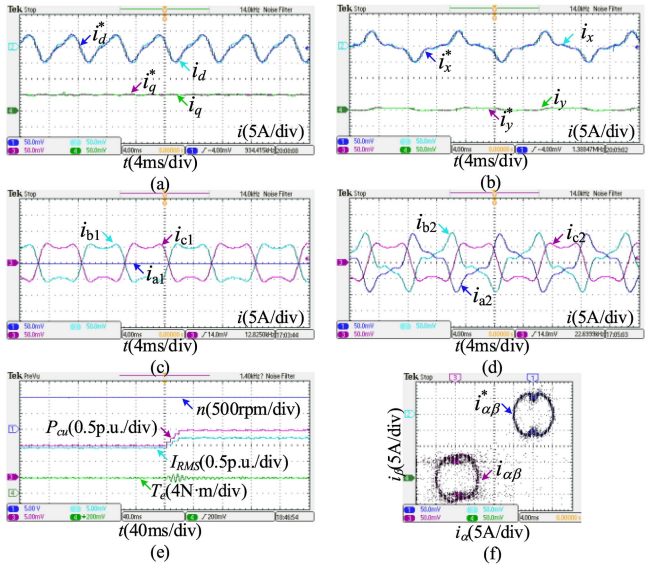

Fig. 11. MT-based experimental results for two isolated neutrals configuration. Current waveforms on (a) d-q subspace; (b) x-y subspace; (c) a_1-b_1-c_1 reference frame; (d) a_2-b_2-c_2 reference frame; (e) speed, torque, copper loss, and maximum rms current waveforms under healthy state and fault-tolerant state; (f) current trajectory on α-β subspace.

shown in (6), two resonant controllers with center frequencies $2\omega_0$ and $4\omega_0$ are employed to track the second and fourth harmonic components, respectively. Here, ω_0 is the fundamental rotor electrical speed. From (8) and (9), x-y-o_1-o_2 current references contain fundamental, third and fifth harmonic components, which are regulated through resonant controllers with center frequencies ω_0, $3\omega_0$ and $5\omega_0$, respectively. Table V lists the parameters of speed and current controllers.

A. Steady-State Operation

In steady-state operation, the DTP machine without and with a_1-phase open is running at 1000 r/min under about 4 N·m load, i.e., 66.67% of rated load.

Figs. 10 and 11 show experimental results under two isolated neutrals configuration for ML and MT modes, respectively. From Fig. 10(a), the harmonics have been successfully injected into d-axis current. And the x-y current waveforms in Fig. 10(b) and phase current waveforms in Fig. 10(c)–(d) are consistent with the theoretical ML-based current waveforms in Fig. 5. The speed, torque, copper loss and maximum rms current waveforms under healthy state and ML-based fault-tolerant state are given in Fig. 10(e), where smooth torque and speed can be obtained due to the undisturbed q-axis current in Fig. 10(a) for ML mode, although the trajectory of actual α-β currents in Fig. 10(f) is no longer circular. From Fig. 10(e), the normalized copper loss and rms current are about 1.35 p.u. and 1.5 p.u. for ML mode, respectively, which are close to the corresponding theoretical values in Table II. From Fig. 11(a)–(d), both d-q, x-y current waveforms and phase waveforms are consistent with theoretical MT-based current waveforms in Fig. 6. It can be seen from Fig. 11(e)–(f) that MT mode can also provide smooth torque and speed, even under obviously unbalanced α-β currents. From Fig. 11(e), the normalized copper loss and rms current are about 1.5 p.u. and 1.25 p.u. under MT mode, respectively, which are close to the corresponding theoretical values in Table II.

Figs. 12 and 13 show experimental results under single isolated neutral configuration for ML and MT modes, respectively. For ML mode, the current waveforms on d-q, x-y, o_1-o_2 subspaces in Fig. 12(a)–(c) and phase current waveforms in Fig. 12(d)–(e) are consistent with its theoretical current waveforms in Fig. 3. From Fig. 12(f), the smooth torque and speed can be obtained for ML mode, although the corresponding trajectory of actual α-β currents in Fig. 14(b) is no longer circular. From Fig. 12(f), the normalized copper loss and rms current are about 1.25 p.u. and 1.5 p.u. for ML mode, respectively, which are close to the corresponding theoretical values in Table II. From Fig. 13(a)–(e), both d-q, x-y, o_1-o_2 current waveforms and phase waveforms are consistent with the corresponding theoretical waveforms in Fig. 4. It can be seen from Figs. 13(f) and 14(c) that the same smooth torque and speed can be obtained, even under unbalanced α-β currents. From Fig. 13(f), the normalized copper loss and rms current are about 1.4 p.u. and 1.3 p.u. under MT mode, respectively, which are close to the corresponding theoretical values in Table II.

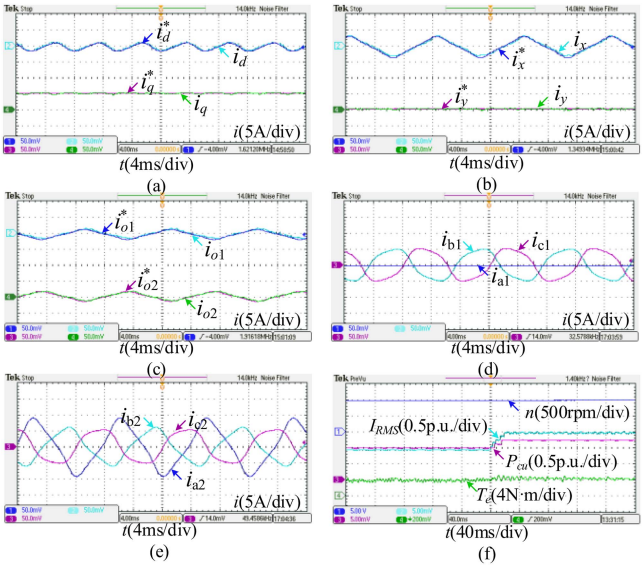

Fig. 12. ML-based experimental results for single isolated neutral configuration. Current waveforms on (a) d-q subspace; (b) x-y subspace; (c) o_1-o_2 subspace; (d) a_1-b_1-c_1 reference frame; (e) a_2-b_2-c_2 reference frame; (f) speed, torque, copper loss and maximum rms current waveforms under healthy state and fault-tolerant state.

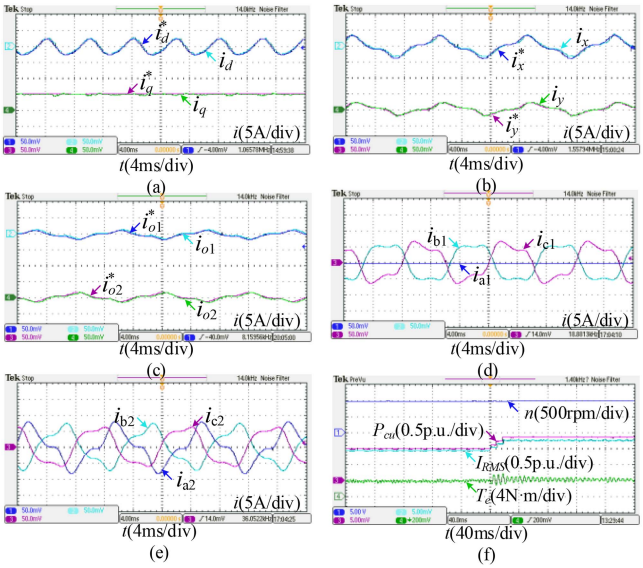

Fig. 13. MT-based experimental results for single isolated neutral configuration. Current waveforms on (a) d-q subspace; (b) x-y subspace; (c) o_1-o_2 subspace; (d) a_1-b_1-c_1 reference frame; (e) a_2-b_2-c_2 reference frame; (f) speed, torque, copper loss and maximum rms current waveforms under healthy state and fault-tolerant state.

Figs. 15 and 16 show experimental results for M0 without harmonic injection and M1–M4 methods with different harmonic injection, respectively. From Fig. 15(a) and (b), for single isolated neutral configuration, the copper losses under ML and MT modes are 1.25 p.u. and 1.7 p.u., respectively, while the maximum rms currents are 1.6 p.u. and 1.25 p.u., respectively. For two isolated neutrals configuration, the copper losses under ML and MT modes are 1.5 p.u. and 1.85 p.u., respectively,

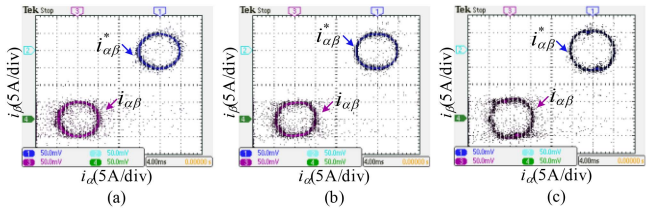

Fig. 14. Current trajectories on α-β subspace for single isolated neutral configuration. (a) Healthy state. (b) ML mode. (c) MT mode.

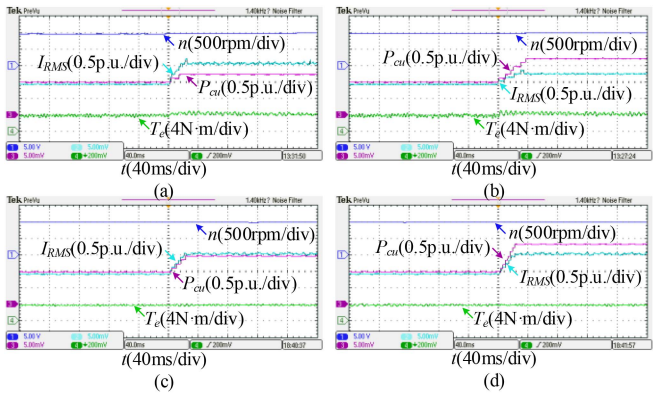

Fig. 15. Experimental results for M0 method without harmonic injection. (a) ML- and (b) MT-based fault-tolerant mode for single isolated neutral configuration. (c) ML- and (d) MT-based fault-tolerant mode for two isolated neutrals configuration.

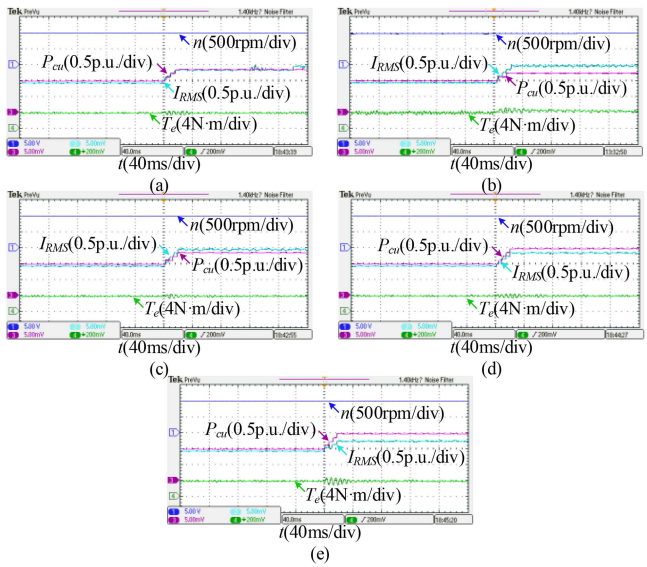

Fig. 16. Experimental results for M1–M4 methods with different harmonic injection. (a) M1 method. M2 method for (b) single and (c) two isolated neutrals configurations. (d) M3 method. (e) M4 method.

while the maximum rms currents are 1.55 p.u. and 1.5 p.u., respectively, as shown in Fig. 15(c) and (d). It can be seen from Fig. 16(a) that the copper loss and maximum rms current of M1 method are 1.35 p.u. and 1.35 p.u., respectively. For M2 method, the copper losses under single and two isolated neutrals

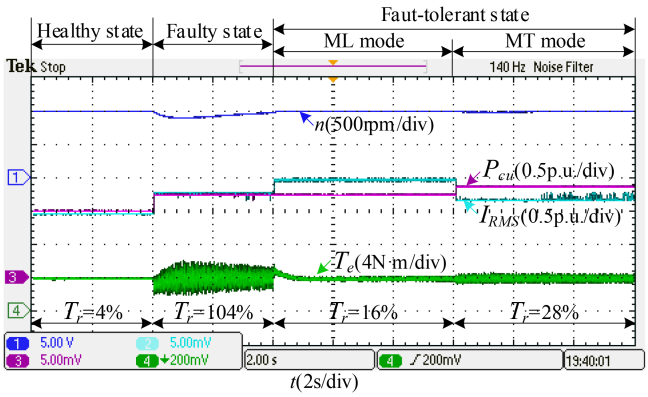

Fig. 17. Experimental results under healthy state, faulty state, ML-, and MT-based fault-tolerant state for single isolated neutral configuration.

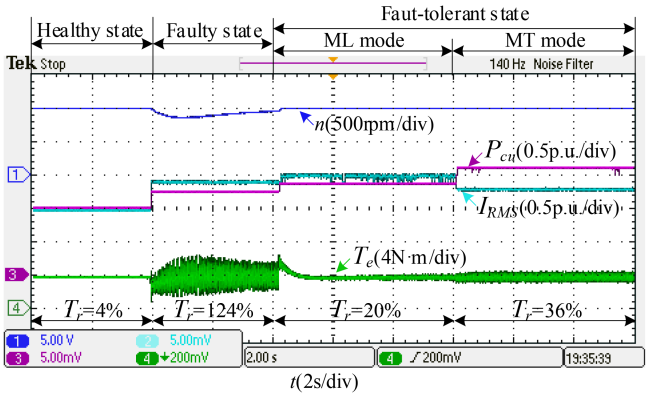

Fig. 18. Experimental results under healthy state, faulty state, ML-, and MT-based fault-tolerant state for two isolated neutral configurations.

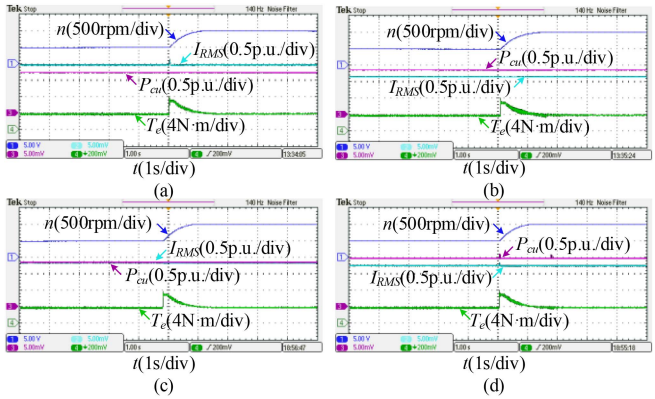

Fig. 19. Experimental results under speed variation. (a) ML- and (b) MT-based fault-tolerant mode for single isolated neutral configuration. (c) ML- and (d) MT-based fault-tolerant mode for two isolated neutrals configuration.

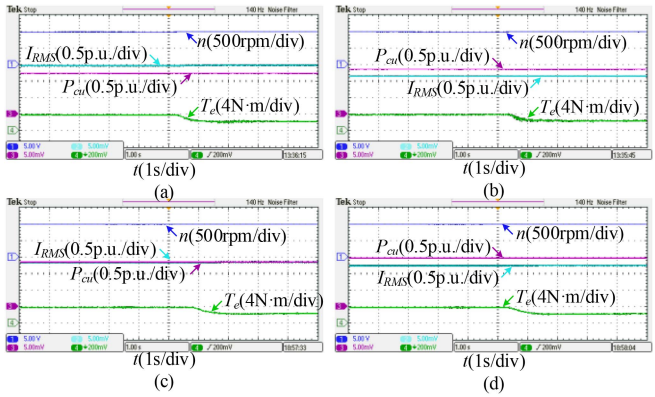

Fig. 20. Experimental results under load variation. (a) ML- and (b) MT-based fault-tolerant mode for single isolated neutral configuration. (c) ML- and (d) MT-based fault-tolerant mode for two isolated neutrals configuration.

configurations are 1.25 p.u. and 1.35 p.u., respectively, while the maximum rms currents are 1.5 p.u., and 1.45 p.u., respectively, as shown in Fig. 16(b) and (c). For M3 and M4 methods, the copper losses are 1.5 p.u., and 1.5 p.u., respectively, while the maximum rms currents are 1.3 p.u. and 1.25 p.u., as shown in Fig. 16(d) and (e). It can be concluded that the M2 method provides lowest copper loss, while M4 method provides the lowest rms current, compared to other methods. Combined with the experimental results shown in Figs. 10–13, the proposed method in this paper provides similar fault-tolerant performance to M2 and M4 methods under ML and MT modes, respectively. All of these are close to the theoretical analysis in Table II.

Figs. 17 and 18 show experimental results under healthy state, faulty stats, ML- and MT-based fault-tolerant state for single and two isolated neutrals configurations, respectively, where the torque ripples T_r is the ratio of the error between maximum torque and minimum torque to the average torque. It can be seen from Fig. 17 that under single isolated neutral configuration, the torque ripples are 4%, 104%, 16%, and 28% for healthy state, faulty state, ML-, and MT-based fault-tolerant state, respectively. As for two isolated neutrals configuration, the torque ripples are 4%, 124%, 20%, and 36% for healthy state, faulty state, ML-, and MT-based fault-tolerant state, respectively, as shown in Fig. 18. These demonstrate the ability of the proposed fault-tolerant method to suppresses the torque ripples induced by open-circuit fault, regardless of neutral point configurations and fault-tolerant operation modes. In addition, ML mode provides lower copper loss, while MT mode provides lower rms current, which corresponds to higher torque capability, even under different neutral point configurations.

B. *Transient-State Operation*

Figs. 19 and 20 show experimental results under speed and load variations, respectively. From Fig. 19, the fault-tolerant performance of the proposed method remains unchanged, even when the speed increases from 500 r/min to 1000 r/min. Similar results can be obtained when the load varies from 4 N·m, i.e., 66.67% of rated load, to 2 N·m, i.e., 33.33% of rated load, as shown in Fig. 20. All of them experimentally verify that the optimal coefficient listed in Table I is independent of operation states.

V. Conclusion

This article proposed a fault-tolerant control based on harmonic current injection for surface-mounted machines to explore the limits of copper loss reduction and torque capability improvement, which is achieved through the vector control framework based on full-order VSD matrix with a release of the requirement on *d*-axis current and a simple modification of other current references except *d*-*q* currents. The contributions of this article are as follow.

1) The x-y-o_1-o_2 current references are generated based on α-β current references through simple linear operations, instead of multiple complex functions required in [26].
2) The optimal coefficient is applicable to any surface-mounted DTP machines and throughout the full operation regions, without parameter dependency.
3) It provides similar fault-tolerant performance to previous works through low-order harmonics, instead of those high frequencies required in [27].
4) Regardless of single or two isolated neutrals configurations, ML and MT modes can be implemented selectively just through modifying the coefficient.

Appendix

Table VI shows the optimization code employed in MATLAB software, where built-in nonlinear optimization functions *fmincon* and *fminimax* are employed to solve the optimization problems for ML and MT modes, respectively, user-defined subfunctions *Pcu*, *Irms*, and *Ifc* are calculated by (14), (17), and (10), respectively. It can be seen from Table VI that under optimization procedure, no additional parameters are required, therefore avoiding tuning works.

TABLE VI
Optimization Code Employed in MATLAB Software

	variable	*description*
Input:	*obj*	*The selection of optimization objective. 0 is for ML mode; 1 is for MT mode.*
	neu	*The selection of neutral configuration. 2 is for two isolated neutrals configuration.*
	phif	*The selection of faulty phase angle. 0, 2π/3, -2π/3, π/6, 5π/6, -π/2 are for faulty phase a_1, b_1, c_1, a_2, b_2, c_2, respectively.*

```
%% main function
x0 = zeros(10,1);
Aeq = [];beq = []; %Aeq·x=beq
if neu == 2 %two isolated neutral configuration: k31=k32=0
    Aeq = [Aeq;zeros(1,4) 1 zeros(1,5);zeros(1,5) 1 zeros(1,4)];
    beq = [beq;0;0];
end

if obj == 0 % ML mode
        x = fmincon(@Pcu,x0,[],[],Aeq,beq,[],[],@nonlcon);
elseif obj == 1 % MT mode
        x = fminimax(@Irms,x0,[],[],Aeq,beq,[],[],@nonlcon);
end

%% nonlinear constraint
function [c,ceq] = nonlcon(x)
   c= [];ceq = @Ifc;
end
```

Output:	$x = [k_{11}, k_{12}, k_{21}, k_{22}, k_{31}, k_{32}, k_{d2}, k_{d4}, \varphi_{d2}, \varphi_{d4}]$

References

[1] A. Salem and M. Narimani, "A review on multiphase drives for automotive traction applications," *IEEE Trans. Transp. Electrific.*, vol. 5, no. 4, pp. 1329–1348, Dec. 2019.

[2] E. Levi, "Advances in converter control and innovative exploitation of additional degrees of freedom for multiphase machines," *IEEE Trans. Ind. Electron.*, vol. 63, no. 1, pp. 433–448, Jan. 2016.

[3] M. J. Duran and F. Barrero, "Recent advances in the design, modeling, and control of multiphase machines—Part II," *IEEE Trans. Ind. Electron.*, vol. 63, no. 1, pp. 459–468, Jan. 2016.

[4] A. G. Yepes, I. Gonzalez-Prieto, O. Lopez, M. J. Duran, and J. Doval-Gandoy, "A comprehensive survey on fault tolerance in multiphase ac drives, part 2: Phase and switch open-circuit faults," *Machines*, vol. 10, no. 3, Mar. 2022, Art. no. 221.

[5] J. R. Fu and T. A. Lipo, "Disturbance-free operation of a multiphase current-regulated motor drive with an opened phase," *IEEE Trans. Ind. Appl.*, vol. 30, no. 5, pp. 1267–1274, Sep./Oct. 1994.

[6] N. Bianchi, S. Bolognani, and M. Dai Pre, "Strategies for the fault-tolerant current control of a five-phase permanent-magnet motor," *IEEE Trans. Ind. Appl.*, vol. 43, no. 4, pp. 960–970, July/Aug. 2007.

[7] A. Mohammadpour and L. Parsa, "Global fault-tolerant control technique for multiphase permanent-magnet machines," *IEEE Trans. Ind. Appl.*, vol. 51, no. 1, pp. 178–186, Jan/Feb. 2015.

[8] W. Li, G. Feng, Z. Li, J. Tjong, and N. C. Kar, "Multireference frame based open-phase fault modeling and control for asymmetrical six-phase interior permanent magnet motors," *IEEE Trans. Power Electron.*, vol. 36, no. 10, pp. 11712–11725, Oct. 2021.

[9] F. Baneira, J. Doval-Gandoy, A. G. Yepes, Ó. López, and D. Pérez-Estévez, "Control strategy for multiphase drives with minimum losses in the full torque operation range under single open-phase fault," *IEEE Trans. Power Electron.*, vol. 32, no. 8, pp. 6275–6285, Aug. 2017.

[10] H. M. Ryu, J. W. Kim, and S. K. Sul, "Synchronous-frame current control of multiphase synchronous motor under asymmetric fault condition due to open phases," *IEEE Trans. Ind. Appl.*, vol. 42, no. 4, pp. 1062–1070, Jul./Aug. 2006.

[11] C. Zhou, W. Tang, X. Sun, Z. Zhou, G. Yang, and J. Su, "Control strategy for dual three-phase PMSM based on reduced order mathematical model under fault condition due to open phases," *J. Eng.*, vol. 2018, pp. 489–494, Apr. 2018.

[12] L. Cheng, Y. Sui, P. Zheng, P. Wang, and F. Wu, "Implementation of postfault decoupling vector control and mitigation of current ripple for five-phase fault-tolerant PM machine under single-phase open-circuit fault," *IEEE Trans. Power Electron.*, vol. 33, no. 10, pp. 8623–8636, Oct. 2018.

[13] B. Tian, Q. T. An, J. D. Duan, D. Y. Sun, L. Sun, and D. Semenov, "Decoupled modeling and nonlinear speed control for five-phase PM motor under single-phase open fault," *IEEE Trans. Power Electron.*, vol. 32, no. 7, pp. 5473–5486, Jul. 2017.

[14] Y. Hu, Z. Q. Zhu, and Z. Y. Wu, "Modelling and vector control of dual three-phase PMSM with one-phase open," *IET Electric. Power Appl.*, vol. 15, pp. 847–860, Mar. 2021.

[15] H. Zhou, W. Zhao, G. Liu, R. Cheng, and Y. Xie, "Remedial field-oriented control of five-phase fault-tolerant permanent-magnet motor by using reduced-order transformation matrices," *IEEE Trans. Ind. Electron.*, vol. 64, no. 1, pp. 169–178, Jan. 2017.

[16] X. Jiang, W. Huang, R. Cao, Z. Hao, and W. Jiang, "Electric drive system of dual-winding fault-tolerant permanent-magnet motor for aerospace applications," *IEEE Trans. Ind. Electron.*, vol. 62, no. 12, pp. 7322–7330, Dec. 2015.

[17] A. Tani, M. Mengoni, L. Zarri, G. Serra, and D. Casadei, "Control of multiphase induction motors with an odd number of phases under open-circuit phase faults," *IEEE Trans. Power Electron.*, vol. 27, no. 2, pp. 565–577, Feb. 2012.

[18] H. S. Che, M. J. Duran, E. Levi, M. Jones, W. Hew, and N. A. Rahim, "Postfault operation of an asymmetrical six-phase induction machine with single and two isolated neutral points," *IEEE Trans. Power Electron.*, vol. 29, no. 10, pp. 5406–5416, Oct. 2014.

[19] I. González-Prieto, M. J. Duran, and F. J. Barrero, "Fault-tolerant control of six-phase induction motor drives with variable current injection," *IEEE Trans. Power Electron.*, vol. 32, no. 10, pp. 7894–7903, Oct. 2017.

[20] W. N. W. A. Munim, M. J. Duran, H. S. Che, M. Bermúdez, I. González-Prieto, and N. A. Rahim, "A unified analysis of the fault tolerance capability in six-phase induction motor drives," *IEEE Trans. Power Electron.*, vol. 32, no. 10, pp. 7824–7836, Oct. 2017.
[21] J. Sun, Z. Liu, Z. Zheng, and Y. Li, "An online global fault-tolerant control strategy for symmetrical multiphase machines with minimum losses in full torque production range," *IEEE Trans. Power Electron.*, vol. 35, no. 3, pp. 2819–2830, Mar. 2020.
[22] M. Shamsi-Nejad, B. Nahid-Mobarakeh, S. Pierfederici, and F. Meibody-Tabar, "Fault tolerant and minimum loss control of double-star synchronous machines under open phase conditions," *IEEE Trans. Ind. Electron.*, vol. 55, no. 5, pp. 1956–1965, May 2008.
[23] W. Wang, J. Zhang, M. Cheng, and S. Li, "Fault-tolerant control of dual three-phase permanent-magnet synchronous machine drives under open-phase faults," *IEEE Trans. Power Electron.*, vol. 32, no. 3, pp. 2052–2063, Mar. 2017.
[24] G. Feng, C. Lai, W. Li, J. Tjong, and N. C. Kar, "Open-phase fault modeling and optimized fault-tolerant control of dual three-phase permanent magnet synchronous machines," *IEEE Trans. Power Electron.*, vol. 34, no. 11, pp. 11116–11127, Nov. 2019.
[25] G. Feng, C. Lai, W. Li, Y. Han, and N. C. Kar, "Computation-efficient solution to open-phase fault tolerant control of dual three-phase interior PMSMs with maximized torque and minimized ripple," *IEEE Trans. Power Electron.*, vol. 36, no. 4, pp. 4488–4499, Apr. 2021.
[26] X. Wang, Z. Wang, M. He, Q. Zhou, X. Liu, and X. Meng, "Fault-tolerant control of dual three-phase PMSM drives with minimized copper loss," *IEEE Trans. Power Electron.*, vol. 36, no. 11, pp. 12938–12953, Nov. 2021.
[27] L. Jin, Y. Mao, X. Wang, P. Shi, L. Lu, and Z. Wang, "Optimization-based maximum-torque fault-tolerant control of dual three-phase PMSM drives under open-phase fault," *IEEE Trans. Power Electron.*, vol. 38, no. 3, pp. 3653–3663, Mar. 2023.
[28] I. G. Prieto, M. J. Duran, P. Garcia-Entrambasaguas, and M. Bermudez, "Field-oriented control of multiphase drives with passive fault tolerance," *IEEE Trans. Ind. Electron.*, vol. 67, no. 9, pp. 7228–7238, Sep. 2020.
[29] X. Wang, Z. Wang, M. Gu, D. Xiao, J. He, and A. Emadi, "Diagnosis-free self-healing scheme for open-circuit faults in dual three-phase PMSM drives," *IEEE Trans. Power Electron.*, vol. 35, no. 11, pp. 12053–12071, Nov. 2020.
[30] R. O. C. Lyra and T. A. Lipo, "Torque density improvement in a six-phase induction motor with third harmonic current injection," *IEEE Trans. Ind. Appl.*, vol. 38, no. 5, pp. 1351–1360, Sep./Oct. 2002.
[31] A. S. Abdel-Khalik, M. I. Masoud, and B. W. Williams, "Improved flux pattern with third harmonic injection for multiphase induction machines," *IEEE Trans. Power Electron.*, vol. 27, no. 3, pp. 1563–1578, Mar. 2012.
[32] A. S. Abdel-Khalik, M. I. Masoud, S. Ahmed, and A. M. Massoud, "Effect of current harmonic injection on constant rotor volume multiphase induction machine stators: A comparative study," *IEEE Trans. Ind. Appl.*, vol. 48, no. 6, pp. 2002–2013, Nov./Dec. 2012.
[33] K. Wang, "Effects of harmonics into magnet shape and current of dual three-phase permanent magnet machine on output torque capability," *IEEE Trans. Ind. Electron.*, vol. 65, no. 11, pp. 8758–8767, Nov. 2018.
[34] T. Wang, L. Guo, K. Wang, J. Wu, C. Liu, and Z. Zhu, "Generalized predictive current control for dual-three-phase PMSM to achieve torque enhancement through harmonic injection," *IEEE Trans. Power Electron.*, vol. 38, no. 5, pp. 6422–6433, May 2023.

Lingling Guo received the B.Eng. and M.S. degrees in automation and control science and engineering from Zhejiang Sci-Tech University, Hangzhou, China, in 2017 and 2020, respectively. She is currently working toward the Ph.D. degree in electrical engineering from Nanjing University of Aeronautics and Astronautics, Nanjing, China.

Her current research interests include fault diagnosis and fault-tolerant control strategies of permanent magnet machine drivers.

K. Wang (Senior Member, IEEE) received the B.Eng. degree in automation engineering from China Jiliang University, Hangzhou, China, in 2004, and the Ph.D. degree in electrical engineering from Zhejiang University, Hangzhou, China, in 2009.

From 2009 to 2010, he was a Postdoctoral Fellow with the Memorial University of Newfoundland, St. John's, NL, Canada. From 2010 to 2013, he was with The University of Sheffield, Sheffield, U.K. From 2013 to 2015, he was a Research Associate with the Sheffield Siemens Wind Power Research Centre, Sheffield, U.K., and a Research and Development Engineer with Ansys Inc., Canonsburg, PA, USA. Since 2015, he has been a Full-Time Professor with the College of Automation Engineering, Nanjing University of Aeronautics and Astronautics, Nanjing, China. His current research interests include the design and control of permanent magnet machines.

Tao Wang (Member, IEEE) received the B.Eng. and Ph.D. degrees in electrical engineering from the College of Electrical Engineering, Zhejiang University, Hangzhou, China, in July 2013 and June 2018, respectively.

From 2018 to 2020, he was a Postdoc Research Associate in the Department of Electronic and Electrical Engineering, The University of Sheffield, U.K. Since 2020, he has been with Nanjing University of Aeronautics and Astronautics, Nanjing, China, where he works as an Associate Professor in the college of automation engineering. His current research interests include wind power generation, aviation power supply, permanent magnet synchronous machine control, and model predictive control.

Ruiwu Cao (Senior Member, IEEE) received the M.S. and Ph.D. degrees in electrical engineering from Southeast University, Nanjing, China, in 2007 and 2013, respectively.

From August 2010 to November 2011, he was a Joint Ph.D. Student with the College of Electrical and Computer Science, University of Michigan-Dearborn, Dearborn, MI, USA, funded by China Scholarship Council. Since 2013, he has been with the Nanjing University of Aeronautics and Astronautics, Nanjing, China, where he is a Professor with the Department of Electrical Engineering. His teaching and research interests include linear motors for rail transit and electromagnetic launch system, motor drives for electric vehicles, and renewable energy generation.

Feng Li received the B.S. degree from the Wanfang College of Science and Technology, Jiaozuo, China, in 2012, the M.S. degree from Henan Polytechnic University, Jiaozuo, China, in 2015, and the Ph.D. degree from Nanjing University of Aeronautics and Astronautics, Nanjing, China, in 2021, all in electrical engineering.

Since 2021, he has been a Postdoc with Nanjing University of Aeronautics and Astronautics. His research interests include the design and control of permanent magnet machines.